Effect of Ambient Temperature Variation on Pressure Drop During Condensation in Long Inclined Tubes

Kaipo Kekaula
Department of Mechanical Engineering,
University of Nevada, Las Vegas,
4505 S. Maryland Parkway,
Las Vegas, NV 89154
e-mail: kaipo.kekaula@unlv.edu

Yitung Chen[1]
Department of Mechanical Engineering,
University of Nevada, Las Vegas,
4505 S. Maryland Parkway,
Las Vegas, NV 89154
e-mail: yitung.chen@unlv.edu

Two-phase flow pressure drop during condensation of steam inside inclined tube heat exchangers was investigated over a wide range of ambient temperature. The ambient temperature changes from 3 to 45 °C, the steam mass flux varies from 3 to 18 kg/(m^2 · s), vapor quality ranges from 0.51 to 0.86. 608 data points were experimentally obtained and compared with eight commonly used correlations from the available literatures. Frictional pressure drop increases with increasing temperature difference and fan speed. For the full experimental dataset, the best overall performing correlation was obtained by using the Wallis correlation (MAPE = 17.60%, NRMSE = 14.87%). For cold ambient temperatures, (T_{amb} < 20 °C, N = 298), the best overall performing correlation was obtained by using the Carey correlation (MAPE = 11.02%, NRMSE = 14.71%). For hot ambient temperatures (T_{amb} > 30 °C, N = 196), the Lockhart and Martinelli correlation has shown the best performance (MAPE = 16.84%, NRMSE = 20.45%). An improved two-phase frictional pressure drop correlation based on the Wallis correlation (Wallis, 1969, One Dimensional Two-Phase Flow, McGraw-Hill, New York) is proposed. [DOI: 10.1115/1.4051070]

Keywords: condensation, heat and mass transfer, heat exchangers, two-phase flow and heat transfer

1 Introduction

Industry focus on water conservation combined with continued concern over the environmental effects of once-through and evaporative cooling has increased interest in air-cooled condensers (ACCs) for the rejection of waste heat in solar thermal power plants. While these systems can reduce the water consumption by up to 90–95%, they experience an average performance penalty when compared with wet and hybrid cooling systems on the order of 3–4% at the plant level [1]. This loss of efficiency is largely caused by the inherent sensitivity of ACC systems to changes in ambient temperature which can reduce power output by 10–20% on the hottest days of the year [2]. Characterizing one of the most fundamental design parameters, pressure drop, over a wide range of ambient temperature conditions is therefore an important component in improving the technology.

Conventional ACC systems are designed in an A-frame configuration. In this setup, steam enters the parallel tube bundles from a large manifold at the top of the condenser. Finned circular tubes or flat tubes are the common types of tubes employed. Air flow is directed over the tubes by a large fan at the bottom of the condenser in a cross-flow manner. The removal of heat from the tubes results in the condensation of the steam, which in liquid form collects at the bottom of the condenser. The low heat transfer coefficients and low mass flux of the condenser tubes typically result in the flow regime within the pipes to be stratified or stratified wavy.

Condensation pressure drop in tubes has been investigated by various research groups in recent years under a range of tube orientation, tube geometry, mass flux, heat transfer, inlet vapor quality, saturation temperature, and pressure. In a two part paper, Lips and Meyer [3] investigated the effect of inclination on pressure drops during condensation of R134a in smooth horizontal and inclined tubes at a saturation temperature of 40 °C. They found that generalized pressure drop correlations had good agreement with vertical upward flows but no correlation predicted downward flows.

Adelaja et al. [4] performed an experimental investigation of pressure drop in a copper tube at various inclination angles and saturation temperatures. They concluded that increases in saturation temperature reduce the interfacial shear leading to a decrease in frictional pressure drop. Noori Rahim Abadi et al. [5] numerically investigated the effects of inclination angle on the heat transfer and pressure drop during condensation of steam in long, smooth, inclined tubes using the volume of fluid (VOF) multiphase flow method in ANSYS FLUENT. Recently, Ewim and Meyer [6] conducted a study of pressure drop during condensation of R134a at low mass fluxes in smooth horizontal and inclined tubes at a saturation temperature of 40 °C.

Due to the challenges associated with predicting pressure drop in inclined tubes, Zendehboudi and Li [7] presented four universal intelligent models, particle swarm optimization-artificial neural network (PSO-ANN), genetic algorithm-least square support vector machine (GA-LSSVM), hybrid approach-adaptive neuro fuzzy inference system (Hybrid-ANFIS), and genetic algorithm-power law committee with intelligent systems (GA-PLCIS) to estimate total and frictional pressure drop. They found that GA-LSSVM, Hybrid-ANFIS, and GA-PLCIS models provided good solution accuracy with GA-PLCIS having the best performance.

Kang and Kim [8] experimentally investigated the impact of inclination on pressure drop for condensation in flat tubes at low mass fluxes. Steam with mass flux of about 7 kg/(m^2 · s) was condensed inside a 10.7 m long, flattened test tube with inclination angle varied from horizontal up to 70 deg. Dalkılıç et al. [9] studied the condensation frictional pressure drop of R134a in smooth and corrugated tubes using 38 correlations from different literatures. The applied mass flux range spans between 709 and 1974 kg/(m^2 · s), the average vapor quality was between 0.09 and 0.97 and the saturation pressure was between 10 and 13 bars.

[1]Corresponding author.

Manuscript received November 8, 2020; final manuscript received April 25, 2021; published online June 18, 2021. Assoc. Editor: Vinod Narayanan.

They found that friction factor modification for corrugated tubes did not improve the overall prediction results for most correlations.

Xu and Fang [10] used experimental data of nine refrigerants with vapor mass flux between 20 and 900 kg/(m$^2 \cdot$ s) and hydraulic diameter from 0.1 to 10.07 mm, and heat flux ranging from 2 to 55.3 kW/m^2 to evaluate the performance of 29 existing pressure drop correlations. They found that the best performing correlation was by Müller-Steinhagen and Heck [11] with a mean absolute relative deviation (MARD) of 25.2%. Kim and No [12] conducted an experimental study of pressure drop in a single vertical tube with an inner diameter of 46 mm at a maximum pressure of 7.5 MPa and found that the predictions of the modified Nusselt theory proposed by Carey [13] underpredicted the total pressure drop.

Didi et al. [14] compared their experimental pressure drop results during the evaporation of refrigerants in smooth horizontal tubes with seven different correlations available in the literatures. Five different refrigerants were used for a total of 788 data points obtained. They concluded that the best predictions for annular flows were given by the correlation of Müller-Steinhagen and Heck [11] and the best predictions for intermittent and wavy flows were given by the correlation of Grönnerud [15]. Wang et al. [16] experimentally investigated frictional pressure drop of steam condensation flow in vacuum horizontal with steam saturation temperature ranging from 50 to 70 °C, and the steam mass flux varying from 2 to 10 kg/(m$^2 \cdot$ s). They compared 205 data points with 25 existing pressure drop correlations and found that the frictional pressure drop increases with vapor quality and mass flux and decreases with saturation temperature.

Despite numerous studies on two-phase flow condensation pressure drop and heat transfer, few are applicable to ACC systems and literature on inclined tubes is still uncommon [17]. In addition to relatively few studies matching the geometric and flow characteristics of ACCs, to the authors knowledge there have been no studies explicitly addressing the impact of a wide range of ambient temperature conditions on the prediction of pressure drop in condenser tubes and no generalized model has been accepted by the research community [18]. The objective of this study is therefore to experimentally investigate the phenomena of steam condensation in inclined tubes in the stratified and stratified-wavy flow regime and to analyze the applicability of various pressure drop correlations from available literatures and then to develop an improved two-phase frictional pressure drop correlation.

2 Pressure Drop Correlations

Experimental data for condensing flows are often compared with correlations derived from databases of adiabatic pressure drop. Due to the fundamental importance of pressure drop on the characteristics and design of condenser systems, numerous methods have been proposed to model the flow pressure drop.

2.1 Homogeneous. The simplest approximation of two-phase flow in tubes is the idealization of homogeneous flow, which assumes that the liquid and vapor phase have the same velocity with mixed physical properties. The combined frictional pressure drop for the mixture is calculated as follows:

$$\left(\frac{\Delta p}{\Delta L}\right)_{fric} = \frac{G^2}{2D\rho_{tp}} f_{tp} \tag{1}$$

where G is the mass flux, ρ_{tp} is the two-phase density of the mixture, and D is the diameter. The two-phase friction factor is then calculated according to following equations for single-phase flow:

$$f_{tp} = \frac{64}{\mathrm{Re}_{tp}} \text{ for } \mathrm{Re}_{tp} < 2100 \tag{2}$$

$$f_{tp} = \frac{0.316}{\mathrm{Re}_{tp}^{0.25}} \text{ for } \mathrm{Re}_{tp} > 2100 \tag{3}$$

where two-phase Reynolds number, Re_{tp} is defined as

$$\mathrm{Re}_{tp} = \frac{GD}{\mu_{tp}} \tag{4}$$

The two-phase density ρ_{tp} and two-phase viscosity μ_{tp} are calculated as follows:

$$\rho_{tp} = \left(\frac{1-x}{\rho_l} + \frac{x}{\rho_v}\right)^{-1} \tag{5}$$

$$\mu_{tp} = (\alpha_l \mu_l + (1-\alpha_l)\mu_v)^{-1} \tag{6}$$

where x is the vapor quality. Homogeneous models are differentiated by their calculation of μ_{tp} and many correlations have been proposed.

2.2 Separated ϕ_{lv}—Models. Separated flow models treat the liquid and vapor phases as separate domains, which better represents the physical situation. Separated flow models can be broadly subdivided into two categories: ϕ_{lv}—models (liquid-vapor) and ϕ_{lo}—models (liquid-only). ϕ_{lv} models combine both liquid and vapor phase pressure drop with a two-phase multiplier.

$$\left(\frac{\Delta p}{\Delta L}\right)_{fric} = \left(\frac{\Delta p}{\Delta L}\right)_{l} \phi_{lv}^2 \tag{7}$$

$$\left(\frac{\Delta p}{\Delta L}\right)_{l} = \frac{[G(1-x)]^2}{2D\rho_l} f_l \tag{8}$$

$$\mathrm{Re}_l = \frac{G(1-x)D}{\mu_l} \tag{9}$$

where f_l is the liquid friction factor calculated using the liquid physical properties and mass flux. Lockhart and Martinelli [19] initially investigated a ϕ_{lv} pressure drop model based on the assumptions that the static pressure drop of the liquid phase and the gas phase must be equal and the sum of the volume occupied by each phase must be equal to the total volume of the pipe. The graphical results for the two-phase multiplier, ϕ_{lv}^2 presented by Lockhart and Martinelli [19] were later fit to the following algebraic function by Chisholm [20]

$$\phi_{lv}^2 = 1 + \frac{C}{X} + \frac{1}{X^2} \tag{10}$$

where X was termed the Lockhart-Martinelli parameter

$$X = \left[\frac{(\Delta p/\Delta L)_l}{(\Delta p/\Delta L)_v}\right]^{0.5} \tag{11}$$

and C is the flow-dependent Chisholm parameter.

2.3 Separated ϕ_{lo}—Model. The second type of separated pressure drop model is the ϕ_{lo}—model, where frictional pressure drop is the product of the frictional pressure drop of the liquid phase and the two-phase multiplier calculated from the liquid phase

$$\left(\frac{\Delta p}{\Delta L}\right)_{frict} = \left(\frac{\Delta p}{\Delta L}\right)_{lo} \phi_{lo}^2 \tag{12}$$

$$\left(\frac{\Delta p}{\Delta L}\right)_{lo} = \frac{G^2}{2D\rho_l} f_{lo} \tag{13}$$

$$\mathrm{Re}_{lo} = \frac{GD}{\mu_l} \tag{14}$$

where f_{lo} is the liquid-only friction factor calculated by Eqs. (2) and (3) using liquid physical properties and the vapor mass flux. The "liquid-only" two-phase multiplier, varies in definition

based on the model and commonly used defninitions are shown in Table 1.

2.4 Film Thickness—Surface Roughness Analogy. Another method was introduced when Wallis [21] noticed a similarity between frictional pressure drop due to two-phase flow and frictional pressure drop due to surface roughness and suggested a correlation which calculates an effective surface roughness based on film thickness. He fit a set of annular flow experimental data resulting in the relation:

$$f = 0.005\left[1 + 300\left(\frac{\delta}{D}\right)\right] \tag{15}$$

where D is the tube diameter and δ is the film thickness. The related void fraction α is defined as follows:

$$\alpha = 1 - \frac{4\delta}{D} \tag{16}$$

3 Experimental Setup

The experimental ACC schematic used for measuring two-phase pressure drop under ambient conditions is shown in Fig. 1. ACCs are the intersection of two fluid loops, a steam Rankine cycle and an open cooling loop with ambient air. A booster pump circulates water from a 100 gallon tank to a 20 kW steam generator (Sussman T-07603-40). A globe valve and superheater are installed between the steam generator and test section to ensure only steam

Table 1 Frictional pressure drop correlations

Reference	Correlation
Lockhart and Martinelli [19]	$C = 5$ laminar liquid – laminar vapor $C = 10$ turbulent liquid – laminar vapor $C = 12$ laminar liquid – turbulent vapor $C = 20$ turbulent liquid – turbulent vapor
Chisholm [23]	$\phi_{lo}^2 = 1 + (\Gamma^2 - 1)(Bx^{0.875}(1-x)^{0.875} + x^{1.75})$ $B = 4.8\Gamma \le 9.5,\ G \le 500\ \text{kg/m}^2\text{s}$ $B = \frac{2400}{G}\Gamma \le 9.5,\ G < 500 < 1900\ \text{kg/m}^2\text{s}$ $B = \frac{55}{G^{0.5}}\Gamma \le 9.5,\ G \ge 1900\ \text{kg/m}^2\text{s}$ $B = \frac{520}{\Gamma G^{0.5}}\ 9.5 < \Gamma < 28,\ G \le 600\ \text{kg/m}^2\text{s}$ $B = \frac{21}{\Gamma}\ 9.5 < \Gamma < 28,\ G > 600\ \text{kg/m}^2\text{s}$ $B = \Gamma^2 G^{0.5}\ \Gamma \ge 28$
Friedel [24]	$\phi_{lo}^2 = (1-x)^2 + x^2\Gamma^2 + \frac{3.24x^{0.78}(1-x)^{0.224}}{\text{Fr}_{tp}^{0.045}\text{We}_{tp}^{0.035}}\left(\frac{\rho_l}{\rho_g}\right)^{0.91}\left(\frac{\mu_g}{\mu_l}\right)^{0.19}\left(1-\frac{\mu_g}{\mu_l}\right)^{0.7}$ $\rho_{tp} = \left(\frac{x}{\rho_g} + \frac{1-x}{\rho_l}\right)^{-1}\ \text{Fr} = \frac{G^2}{gD\rho_{tp}^2}$
Grönnerud [15]	$\phi_{lo}^2 = 1 + f_{\text{Fr}}[x + 4(x^{1.8} - x^{10}f_{\text{Fr}}^{0.5})]\left[\left(\frac{\rho_l}{\rho_v}\right)\left(\frac{\mu_v}{\mu_l}\right)^{0.25} - 1\right]$ $f_{\text{Fr}} = \text{Fr}_{lo}^{0.3} + 0.0055\left[\ln\left(\frac{1}{\text{Fr}_{lo}}\right)\right]^2;\ \text{Fr}_{lo} < 1$ $f_{\text{Fr}} = 1;\ \text{Fr}_{lo} > 1$
Müller-Steinhagen and Heck [11]	$\phi_{lo}^2 = [1 + 2x(\Gamma^{-2} - 1)](1-x)^{\frac{1}{3}} + \Gamma^2 x^3$
Wallis [21]	$f = 0.005\left[1 + 300\left(\frac{\delta}{D}\right)\right]$ $\alpha = 1 - \frac{4\delta}{d}$
Carey [13]	$f = 0.079\left[\frac{Gx(\text{D}-\delta)}{\mu_g\left(1-\frac{4\delta}{d}\right)}\right]^{-0.25}$ $\alpha = 1 - \frac{4\delta}{D}$

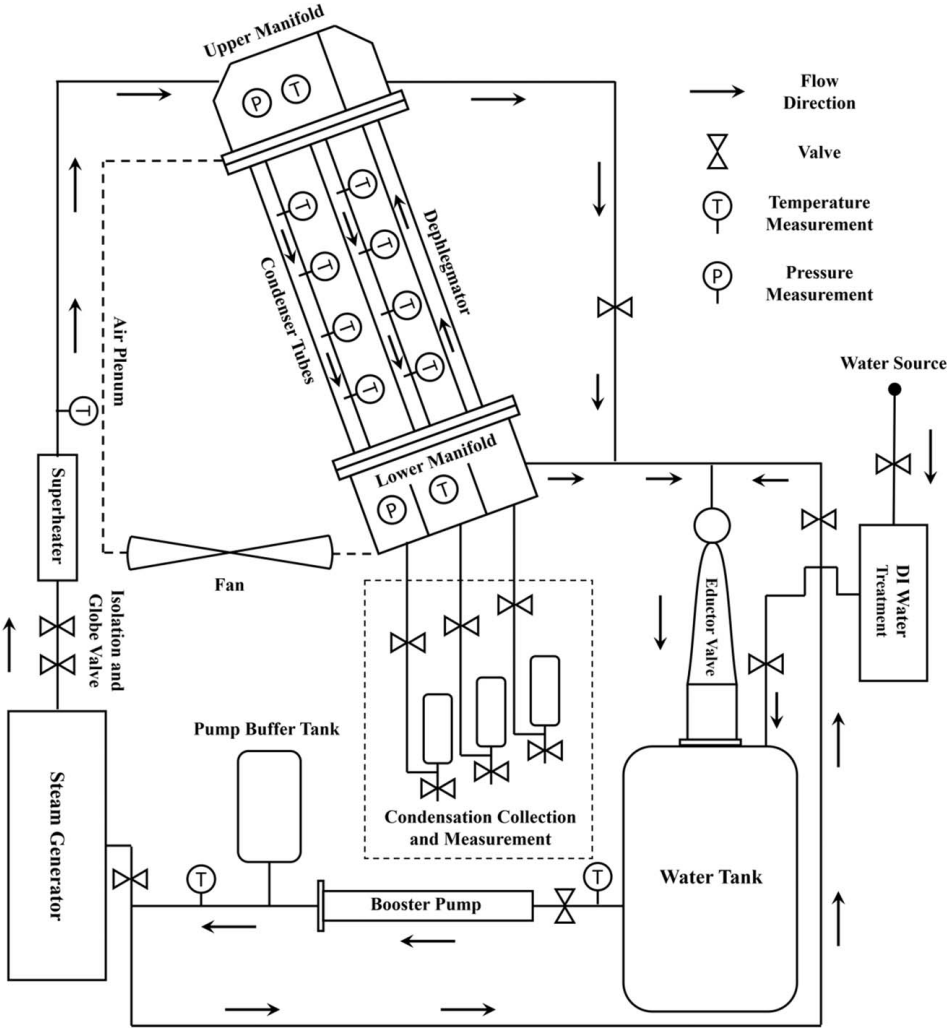

Fig. 1 Schematic diagram of experimental apparatus

vapor enters the test section and to reduce the pressure to near atmospheric. At the lower manifold of the condenser test section, liquid condensate is collected into three tanks. Two collection tanks are dedicated to the tested finned tubes and one is dedicated to the dephlegmator. Excess steam is directed into the tank by an eductor valve, creating a closed loop. The experimental facility is located in the docking area of the Science and Engineering building at the University of Nevada, Las Vegas and shown in Fig. 2. The system is run for 30 min at max capacity before testing to ensure that all of the air is removed from the system.

Cooling air is provided to the test section by an axial fan with a 762 mm diameter and driven by a 559 watt motor. The fan is controlled by a variable frequency drive allowing for precise adjustment of the fan speed. The test section is 6.096 m long and 304.8 mm wide and operates as a cross-flow heat exchanger with steam flowing in finned tubes and ambient air flowing perpendicular to the axial direction of the steam. The five brazed finned copper tubes inclined at 78.8 deg from the horizontal with length, $L = 6.096$ m with inner and outer diameter of the tubes are 14.84 and 15.88 mm, respectively. The fins are 0.51 mm thick with a spacing of 5.1 mm as shown in Fig. 3.

Ambient conditions are measured at the top of the ACC system. Air temperature and relative humidity are measured using a Vaisala HMP60-L temperature and relative humidity probe. Ambient pressure is measured by a CS100 barometric pressure sensor. Ten T-type thermocouples are used to make temperature measurements of the steam loop. The inlet flowrate of the liquid water is measured

Fig. 2 Experimental ACC system

Fig. 3 Brazed finned tubes

using an Omega FTB4707 water flowmeter that has a sensitivity of 1%. The pressure drop is measured by pressure transducers (Omega PX279-05G5V) installed in the upper and lower manifolds. Air temperature and velocity are measured using five Omega FMA-903 air velocity transducers, with four positioned at evenly spaced positions along the length of the test section downflow of the finned tubes and another located at the fan outlet.

4 Data Reduction

The total pressure drop is a combination of three components: the frictional drop, gravitational drop, and momentum pressure drops

$$\Delta P_{total} = \Delta P_{fric} + \Delta P_{stat} + \Delta P_{mom} \tag{17}$$

Momentum pressure drop is determined from the change in kinetic energy from the inlet to the exit caused by the change in density

$$\Delta P_{mom} = G^2 \left\{ \left[\frac{(1-x)^2}{\rho_l(1-\alpha)} + \frac{x^2}{\rho_v \alpha} \right]_e - \left[\frac{(1-x)^2}{\rho_l(1-\alpha)} + \frac{x^2}{\rho_v \alpha} \right]_i \right\} \tag{18}$$

where ρ_v and ρ_l are the vapor and liquid phase density, respectively, x is the vapor quality, α is the void fraction. Static pressure drop due to gravity can be determined from

$$\Delta P_{stat} = g(\alpha \rho_v + (1-\alpha)\rho_l)h \tag{19}$$

where g is gravitational acceleration and h is the change in height between the tube inlet and tube outlet. Mass flux G can be calculated as

$$G = \frac{\dot{m}_{tube}}{A_{tube}} \tag{20}$$

Void fraction, α is calculated from the modified drift flux model of Steiner [22]

$$\alpha = \frac{x}{\rho_v}\left[(1 + 0.12(1-x))\left(\frac{x}{\rho_v} + \frac{1-x}{\rho_l} \right) + \frac{1.18(1-x)[g\sigma(\rho_l - \rho_v)]^{0.25}}{G\rho_l^{0.5}} \right]^{-1}$$

To evaluate the accuracy of each predictive model, three parameters are introduced: the mean percent error (MPE), the mean absolute percent error (MAPE), and the normalized root mean square error (NRMSE)

$$\text{MPE} = \frac{1}{N}\sum_{i=1}^{N} PE_i \times 100\% \tag{21}$$

$$\text{MAPE} = \frac{1}{N}\sum_{i=1}^{N} |PE_i| \times 100\% \tag{22}$$

$$\text{NRMSE} = \left(\frac{1}{S_{exp}} \right)\left(\frac{1}{N}\sum_{i=1}^{N} E_i^2 \right)^{\frac{1}{2}} \times 100\% \tag{23}$$

where error E_i, percent error PE_i, and experimental span S_{exp} are defined as

$$E_i = (\Delta P/\Delta L)_{i,mod} - (\Delta P/\Delta L)_{i,exp} \tag{24}$$

$$PE_i = \frac{(\Delta P/\Delta L)_{i,mod} - (\Delta P/\Delta L)_{i,exp}}{(\Delta P/\Delta L)_{i,exp}} \tag{25}$$

$$S_{exp} = \max\left(\left(\frac{\Delta P}{\Delta L} \right)_{i,exp} \right) - \min\left(\left(\frac{\Delta P}{\Delta L} \right)_{i,exp} \right) \tag{26}$$

Subscripts *exp* and *mod* represent the experimental value and predicted model value, respectively. N is the number of experimental data points.

4.1 Uncertainty Propagation. The measured parameters here are used in the data reduction process and resulting in uncertainty in calculated results. The propagation of this uncertainty can be estimated using the method of Chisholm [23], which uses a mean square error procedure to calculate the system uncertainty from individual components

$$U_F = \left[\left(\frac{\partial F}{\partial x_1} U_1 \right)^2 + \left(\frac{\partial F}{\partial x_2} U_2 \right)^2 + \cdots + \left(\frac{\partial F}{\partial x_n} U_n \right)^2 \right]^{0.5} \tag{27}$$

where $U_1, U_2, \ldots, U_n$ are the uncertainties the independent variables that affect dependent variable, F. The operating conditions and associated uncertainty in measured data are shown in Table 2. From Eq. (27), we find that the uncertainty of the vapor quality, vapor Reynolds number, liquid Reynolds number are, 0.95%, 4.3%, and 6.4%, respectively. The uncertainty for frictional pressure drop was estimated to be between 3.53% and 9.47% for the eight correlations compared in this study.

5 Results and Discussion

The flow characteristics play a significant role in condensation pressure drop. Figure 4 shows the vapor and liquid Reynolds

Table 2 Operating conditions and uncertainty of experimental parameters

Parameter	Range	Uncertainty
Air velocity, V_a (m/s)	0–4.35	±1.0%
Ambient temperature, T_{amb} (°C)	3–45	±0.1
Condensing pressure, P_{sat} (kPa)	95–168	±0.1
Vapor mass flux, G (kg/(m^2 s))	3–18	±1.0%

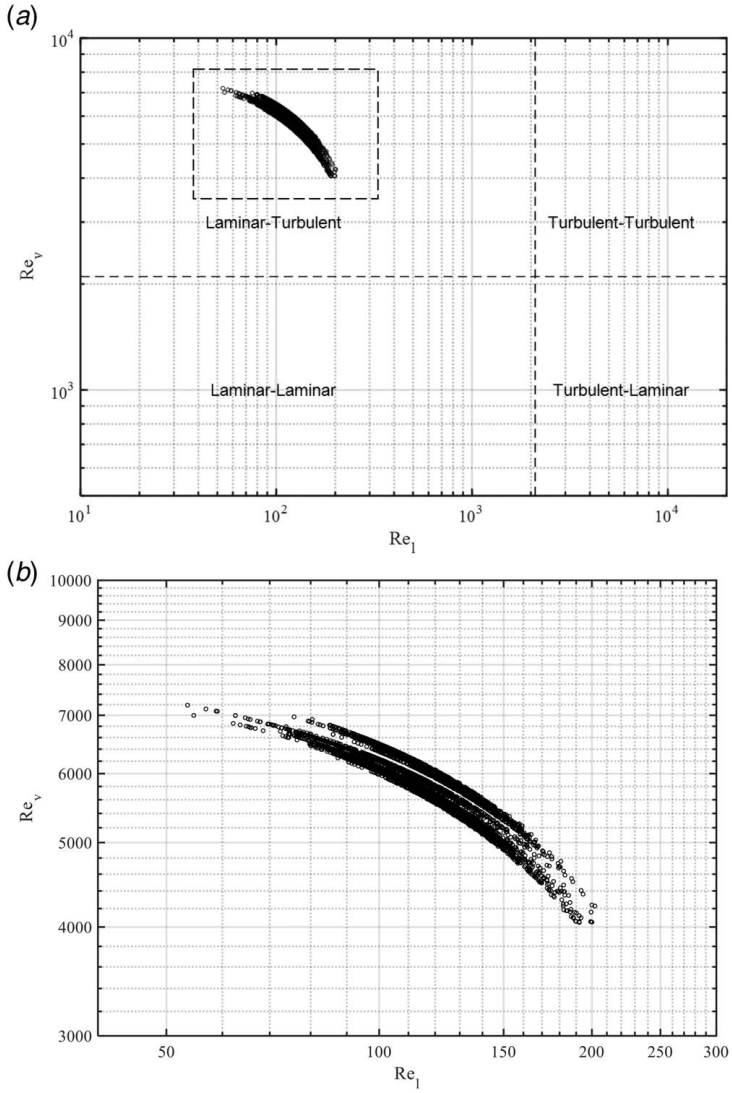

Fig. 4 (*a*) Experimental flow conditions for vapor and liquid phases and (*b*) experimental flow conditions for vapor and liquid phases (enlarged)

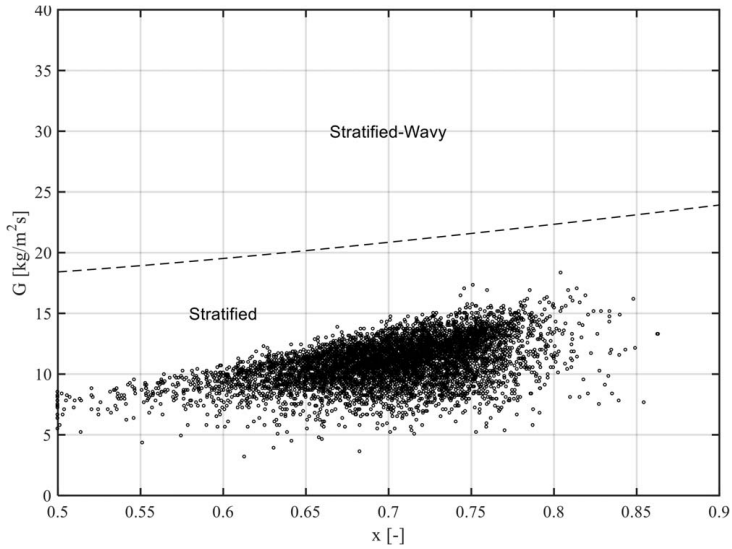

Fig. 5 Experimental data compared with flow pattern map proposed by El Hajal et al. [25]. The dotted line indicates the stratified/stratified-wavy transition and is given by Eq. (28).

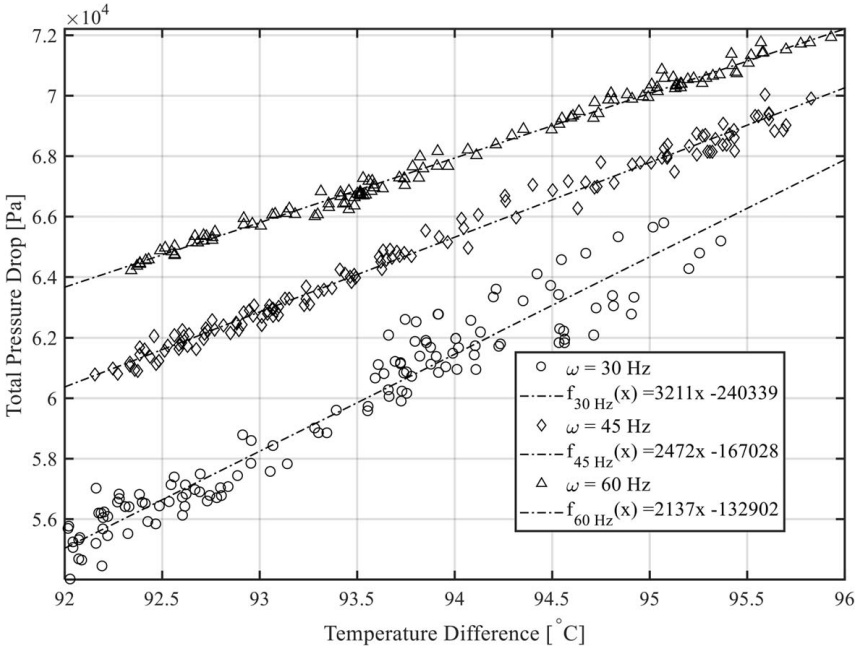

Fig. 6 Variation of total pressure drop with temperature difference with low ambient temperature ($T_{amb} < 20$ °C)

number for the experimental data. The plot is subdivided into four quadrants that indicate whether each phase is in laminar or turbulent flow. The inlet steam mass flux ranges from 3 and 18 kg/(m$^2 \cdot$ s), and the steam saturation temperature ranges from 98 to 109 °C. The flow regime of the vapor and liquid phases of the system both impact the two-phase frictional pressure drop and are implemented in the pressure drop correlations. The vapor mass flux in air-cooled condensers is generally small, but due to the low kinematic viscosity, it will typically be in the turbulent flow regime. The low liquid volume fraction results in a slow moving, gravity driven film along the tube wall which is in the laminar flow regime.

The distribution of the liquid and vapor phases can also have a large impact on the frictional pressure drop. The flow pattern map reported by El Hajal et al. [25] is used to check the flow regime of the experimental data points and plotted in Fig. 5. For flows with low vapor mass flux, flows will typically exist in the stratified and stratified-wavy regime and the transition between these is given by the following equation:

$$G_{strat} = \left[\frac{(226.3)^2 A_l A_v^2 \rho_v (\rho_l - \rho_v)\mu_l g}{x^2(1-x)\pi^3}\right]^{1/3} + 20x \qquad (28)$$

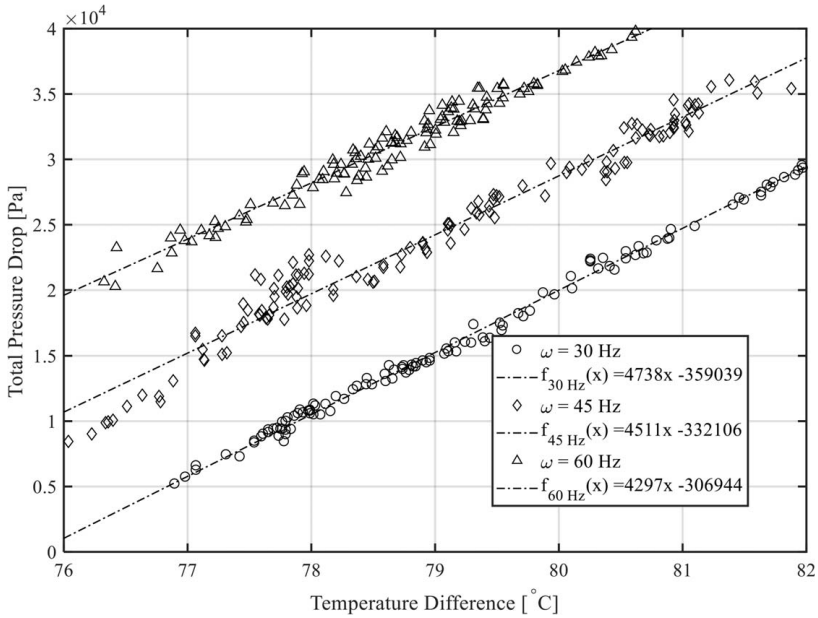

Fig. 7 Variation of total pressure drop with temperature difference with high ambient temperature ($T_{amb} > 30$ °C)

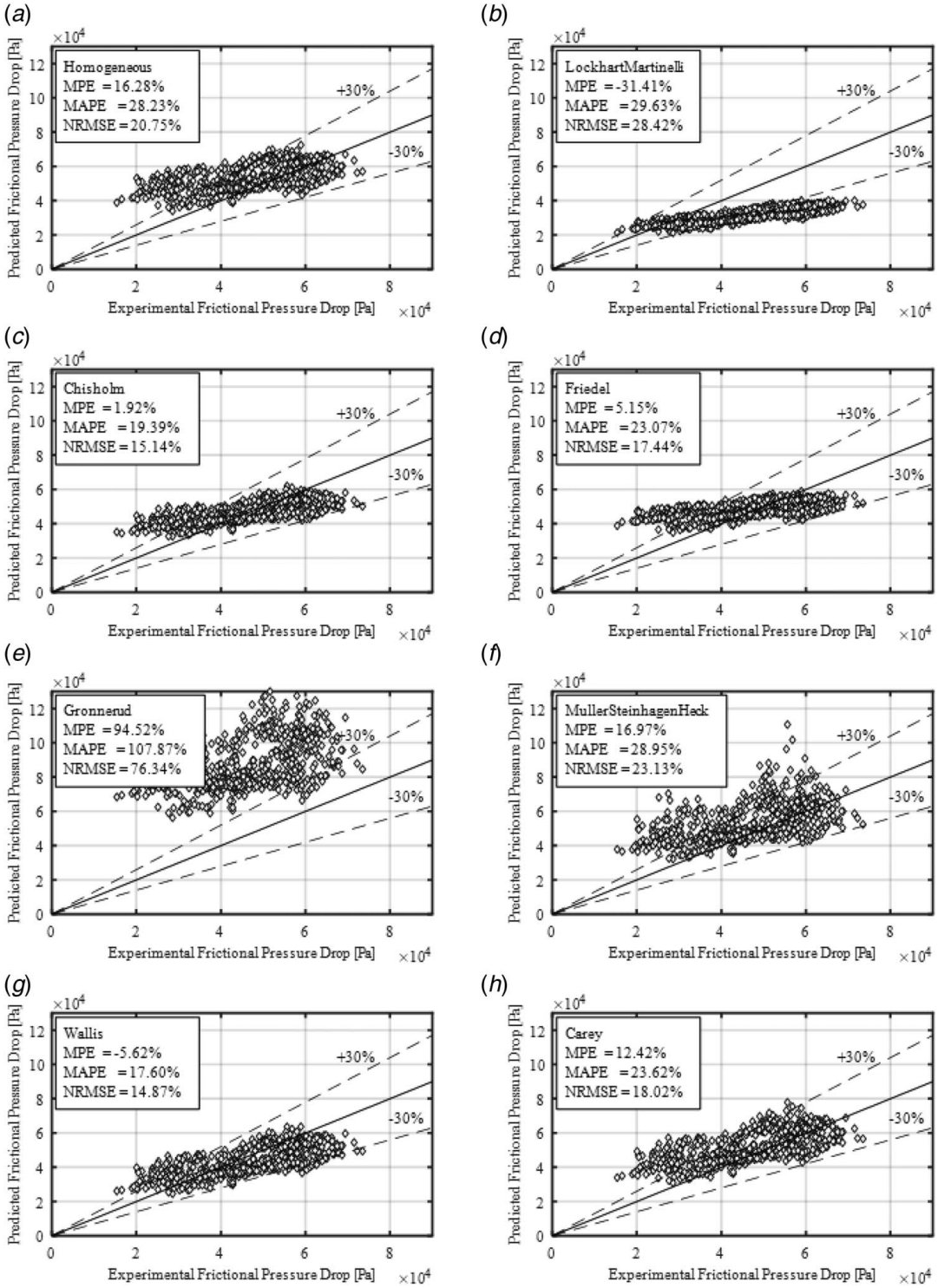

Fig. 8 Comparison of predicted frictional pressure drop with all experimental data

where A_v and A_l are the cross-sectional area of the vapor and liquid flow, respectively

$$A_v = \frac{A\alpha}{D^2} \tag{29}$$

$$A_l = \frac{A(1-\alpha)}{D^2} \tag{30}$$

Figure 6 shows the variation of experimental total pressure drop with temperature difference, ΔT at fan speeds of 30, 45, and 60 Hz and a mean mass flux of 11.5 kg/(m$^2 \cdot$ s) during cold ambient conditions ($T_{amb} < 20$ °C), where ΔT is defined as the saturation temperature, T_{sat} minus the ambient temperature, T_{amb}. From Fig. 6, it is apparent that temperature difference has a significant impact on the total pressure drop. Additionally, it can be seen that for all fan speeds, increases in temperature difference led to a near linear increase in pressure drop. In the stratified flow region, a larger

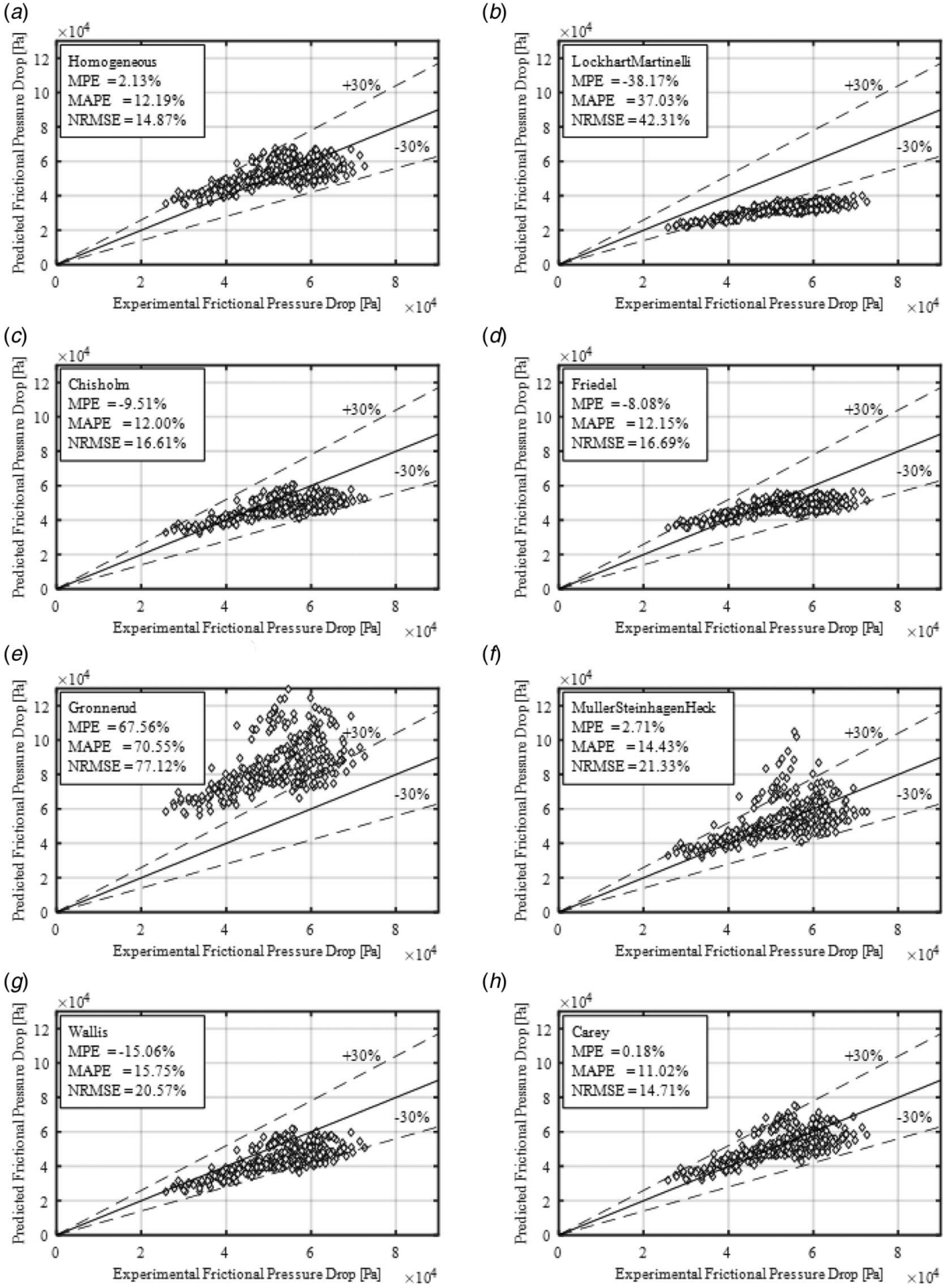

Fig. 9 Comparison of predicted frictional pressure drop with experimental data with low ambient temperature ($T_{amb} < 20$ °C)

temperature difference increases the thickness of the thin film within the condenser tubes and therefore the frictional pressure gradient. This phenomenon is the same as reported by Ewim and Meyer [6]. Figure 7 shows the variation of experimental total pressure drop with temperature difference at fan speeds of 30, 45, and 60 Hz and a mean mass flux of 11.5 kg/(m$^2 \cdot$s) during hot ambient conditions ($T_{amb} > 30$ °C). The average cross-flow air velocity, V_a in the test section was 1.35 m/s when operating the fan at 30 Hz, 1.95 m/s when operating the fan at 45 Hz, and 2.71 m/s when operating the fan at 60 Hz. From Fig. 7, it is again apparent

Table 3 Statistical comparison between the existing correlations and the database

	All ($N = 608$)			Cold extreme ($N = 298$)			Hot extreme ($N = 196$)		
Model/error	MPE (%)	MAPE (%)	NRMSE (%)	MPE (%)	MAPE (%)	NRMSE (%)	MPE (%)	MAPE (%)	NRMSE (%)
Homogeneous	16.28	28.23	20.75	2.13	12.19	14.87	51.07	59.12	48.00
Lockhart and Martinelli [19]	−31.41	29.63	28.42	−38.17	37.03	42.31	−13.99	16.84	20.45
Chisholm [23]	1.92	19.39	15.14	−9.51	12.00	16.61	29.77	36.85	30.76
Friedel [24]	5.15	23.07	17.44	−8.08	12.15	16.69	39.26	47.25	38.46
Grönnerud [15]	94.52	107.87	76.34	67.56	70.55	77.12	153.94	168.47	135.48
Müller-Steinhagen and Heck [11]	16.97	28.95	23.13	2.71	14.43	21.33	47.00	54.51	46.15
Wallis [21]	−5.62	17.60	14.87	−15.06	15.75	20.57	15.33	24.91	21.55
Carey [13]	12.42	23.62	18.02	0.18	11.02	14.71	40.59	47.20	39.42

Table 4 Predictability between the existing correlations and the database

	All ($N = 608$)			Cold extreme ($N = 298$)			Hot extreme ($N = 196$)		
	Predictability (%)			Predictability (%)			Predictability (%)		
Model/error margins	±10%	±20%	±30%	±10%	±20%	±30%	±10%	±20%	±30%
Homogeneous	32.49	57.45	72.41	47.64	81.56	96.13	4.08	20.11	30.37
Lockhart and Martinelli [19]	12.28	19.87	41.20	0.00	1.68	15.75	37.98	57.78	81.57
Chisholm [23]	43.93	69.25	81.42	47.21	80.99	99.06	27.05	35.73	44.10
Friedel [24]	40.36	65.45	78.52	48.38	77.49	97.88	18.22	31.85	38.13
Grönnerud [15]	0.03	0.94	3.59	0.07	2.12	8.45	0.00	0.00	0.00
Müller-Steinhagen and Heck [11]	31.80	55.00	67.42	47.31	77.39	89.84	12.20	23.84	31.50
Wallis [21]	33.09	66.17	86.27	28.84	67.40	94.62	24.20	50.48	65.65
Carey [13]	38.58	62.86	74.88	53.40	85.67	96.67	14.85	27.00	34.10

that temperature difference increases linearly with temperature difference and that for all fan speeds, increases in temperature difference led to an increase in pressure drop.

To further analyze the data, a linear regression was performed at both cold and hot ambient temperature conditions and shown in Figs. 6 and 7. During cold ambient temperatures, the total pressure drop variation with temperature was approximately 3.21, 2.47, and 2.14 kPa/°C for 30, 45, and 60 Hz, respectively. For $\Delta T \cong 94$ °C, increasing the fan speed from 30 to 45 and 60 Hz increases the total pressure drop by about 3.85 kPa (+3.9%) and 6.48 kPa (+6.5%), respectively. During hot ambient temperatures, the total pressure drop variation with temperature was approximately 4.74, 4.51, and 4.30 kPa/°C for 30, 45, and 60 Hz, respectively. For $\Delta T \cong 79$ °C, increasing the fan speed from 30 to 45 and 60 Hz increases the total pressure drop by about 8.97 kPa (+58.9%) and 17.2 kPa (+113%), respectively. From this we can conclude that changes in fan speed have a larger impact on the total pressure drop when the ambient temperature, T_{amb} is high, and the temperature difference is lower. This is because if the inlet vapor mass flux is held constant, when $\Delta T = T_{sat} - T_{amb}$ is high and the air-side thermal resistance is low, the film growth along the inner wall of the condenser tube is limited by the available vapor for condensation.

The frictional pressure drop of the experimental ACC system has been compared with several commonly cited correlations from the available literatures with the goal of establishing the predictability of each model. The predictability of a pressure drop model is the fraction of the total experimental pressure drop database that can be predicted from input parameters within defined accuracy margins, which for this study are ±10%, ±20%, and ±30%. Experimental frictional pressure drop is determined from Eq. (17) by subtracting momentum recovery and gravitational components of the pressure drop from the total pressure drop. For this study, predicted frictional pressure drop is calculated using the mean vapor quality.

The comparison of the entire database of experimental frictional pressure drop with predictions by commonly cited frictional pressure drop models from literature is shown in Fig. 8. A summary of the statistical results for MPE, MAPE, and NRMSE of the correlations from literatures which were calculated according to Eqs. (21)–(23) is shown in Table 3, where N is the number of data points satisfying the temperature criteria. Table 4 shows the predictive ability of each frictional pressure drop for the condensation which is the percentage of data points which were correctly predicted within the indicated ambient temperature condition and error range.

For the full range of ambient temperature conditions, the correlations of Chisholm [23], Friedel [24], Wallis [21], and Carey [13] had the best performance. Best overall performing correlation was Wallis [21] with MAPE of 17.60% and an NRMSE of 14.87%. Of these the correlations of Chisholm [23], Friedel [24], and Carey [13] all over predicted the experimental data while that of Wallis [21] slightly underpredicted. The correlations of Chisholm [23], Friedel [24], and Wallis [21] were all able to predict over 75% of the dataset within ±30% margins with Wallis [21] being the best performer with a predictability of 86.27%. Correlations such as Wallis [21] and Carey [13] have specific reference to film thickness and are therefore more sensitive to changes in vapor void fraction. The method of Grönnerud [15] gave relatively poor predictions of the frictional pressure drop, partially due to the sensitivity of the model two-phase multiplier to vapor quality, x.

The comparison of the colder extreme of the experimental data database ($T_{amb} < 20$ °C, $N = 298$) of experimental frictional pressure drop with literature models is shown in Fig. 9. For this subset, the correlations of Chisholm [23], Friedel [24], Carey [13] and the homogeneous model had the best performance with the best overall performing correlation being Carey [13] with MAPE of 11.02% and an NRMSE of 14.71%. The correlations of Chisholm [23] and Friedel [24] underpredicted the experimental data [13] and the homogeneous model overpredicted. The correlations of Chisholm [23], Friedel [24], and Carey [13] and the homogeneous model all gave acceptable predictions as they were able to predict over 95% of the dataset within 30% with the best being Chisholm [23] with a predictability of 99.06%.

For the hot extreme of the database ($T_{amb} > 30$ °C), the models of Lockhart and Martinelli [19] and Wallis had the best performance.

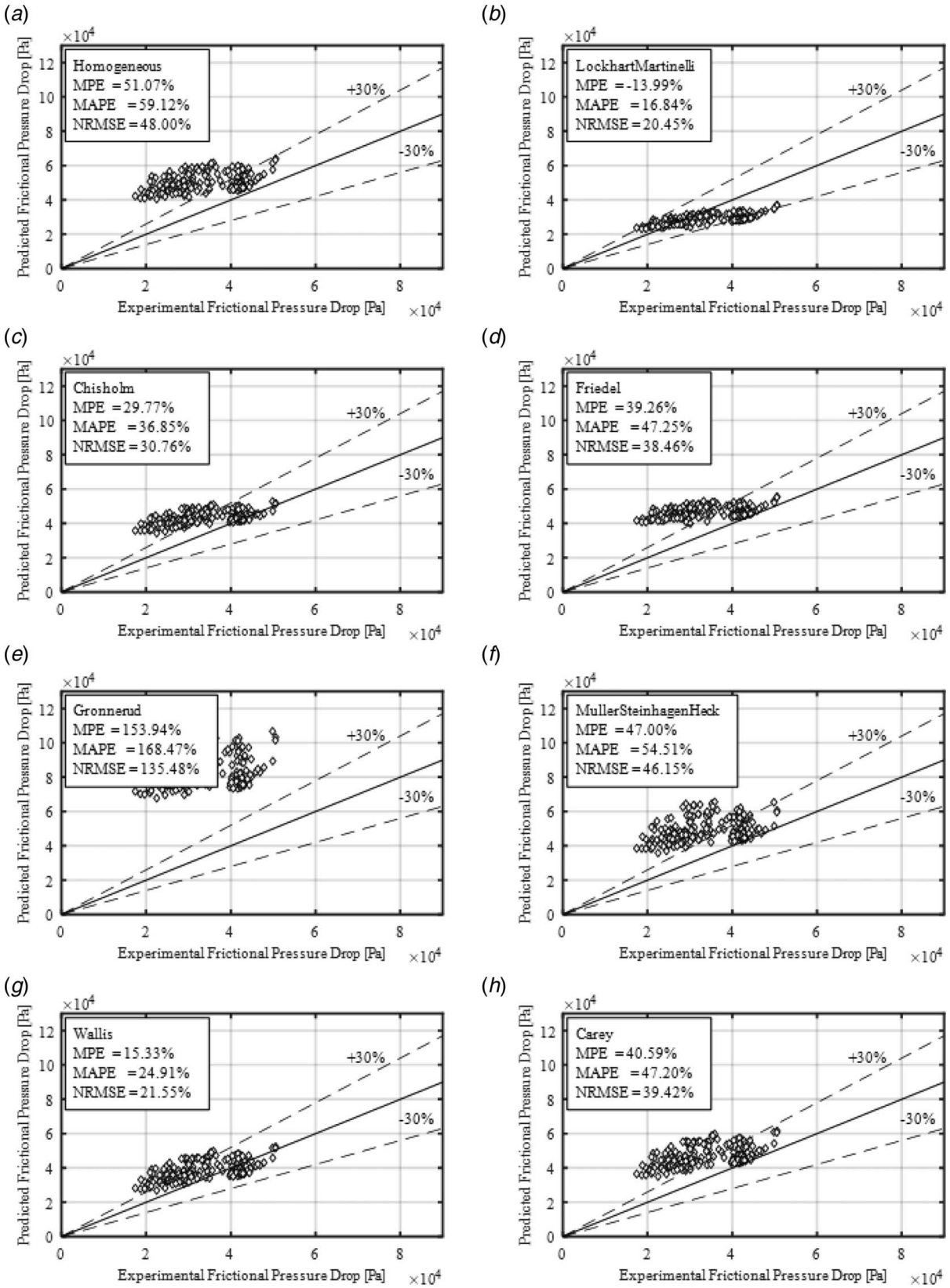

Fig. 10 Comparison of predicted frictional pressure drop with experimental data high ambient temperature (T_{amb} > 30 °C)

Best overall performing correlation was Lockhart and Martinelli [19] with MAPE of 16.84% and an NRMSE of 20.45%, which is shown in Fig. 10. Of these the correlations of Wallis over predicted the experimental data while that of Lockhart and Martinelli [19] slightly underpredicted. The correlations of Lockhart-Martinelli [19] and Wallis [21] were they only models to give acceptable predictions total pressure drop being able to predict 81.57% and 65.65% of dataset within 30%, respectively.

While the pressure drop models were able to give good predictions of the experimental database during low ambient temperature

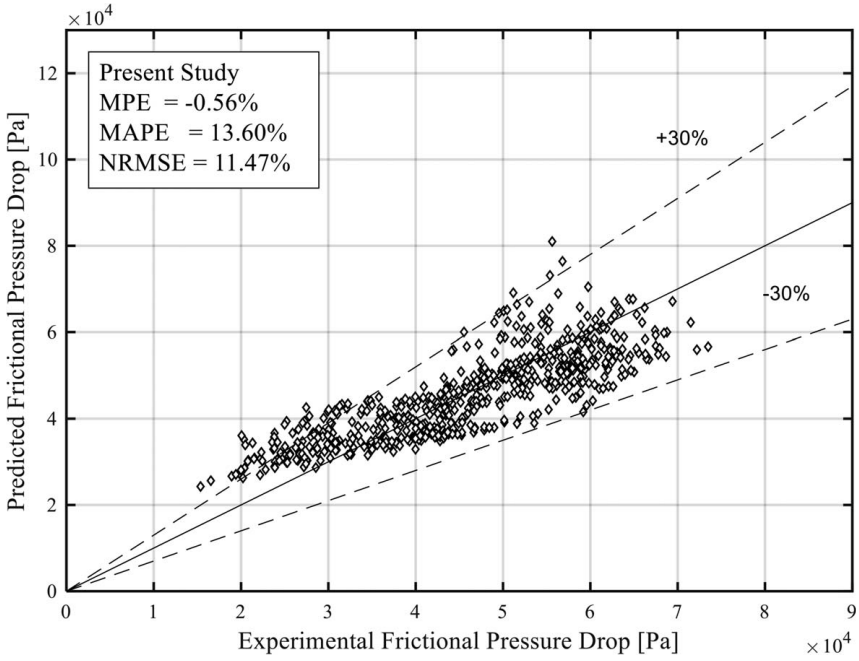

Fig. 11 Comparison of predicted frictional pressure drop using the new correlation with all experimental data

conditions, it is clear that there is much room for improvement when predicting the pressure drop for high ambient temperature conditions. One explanation for the difference in performance is simply that as the ambient temperature decreases, the condensate mass flowrate drops below the range of applicability of the evaluated models. Many of the established correlations have been developed from large databases but the data often become sparse in low liquid mass flux (<20 kg/m^2 s) conditions.

Furthermore, frictional pressure drop correlations typically rely on calculation of multiphase flow parameters ($\alpha, \phi_{lv}, \mu_{tp}$, etc.) from measured bulk physical properties. These mixed phase parameters, while convenient to use, are fairly constant at higher vapor quality due to the high density ratio, ρ_l/ρ_v of water. This insensitivity to variation in the condensate mass flux can result in the overprediction of frictional pressure drop during hot extreme ambient conditions.

6 New Frictional Pressure Drop Correlation

Of the correlations investigated in this study, the Wallis correlation [21] had the best agreement with the experimental database. For this reason, a new correlation was developed based on the film thickness-surface roughness analogy model. The liquid Reynolds number, Re_l was used to correct for the overestimation of frictional pressure drop at low ambient temperatures and the underestimation of friction pressure drop at high ambient temperatures. Applying a nonlinear regression method on the experimental data gives the following relation:

$$f = 0.005\left[1 + 448.4\left(1 + \frac{\mathrm{Re}_l}{821}\right)\left(\frac{\delta}{D}\right)\right]^{0.7586} \tag{31}$$

where D is the tube diameter and δ is the film thickness. Equation (16) is used to calculate the related void fraction α and Eq. (9) is used to calculate the liquid Reynolds number Re_l. Figure 11 shows the comparison of the experimental two-phase frictional pressure drop with the prediction of the new correlation. The current correlation agrees well with the experimental data of T_{amb} < 20 °C and T_{amb} > 30 °C and outperforms all other tested correlations with a MAPE of 16.84% and a NRMSE of 20.45% while being able to predict 91.41% of the entire experimental database within ±30% error margins.

7 Conclusions

This study investigated steam condensation pressure drop in smooth inclined tubes exposed to ambient conditions over a wide range of temperature. The frictional pressure drop was compared with eight commonly cited pressure drop correlations from the available literatures. Changes in fan speed have a larger impact on the total pressure drop when the ambient temperature is high, and the difference between the ambient temperature and saturation temperature, ΔT is lower. For the full range of experimental conditions, the best overall performing correlation was Wallis with MAPE of 17.60% and an NRMSE of 14.87% followed by the correlations of Chisholm [23], Friedel [24], and Carey [13]. For colder extreme of the experimental data database (T_{amb} < 20 °C, N = 298), the best overall performing correlation was Carey [13] with MAPE of 11.02% and an NRMSE of 14.71%, followed by the correlations of Chisholm [23], Friedel [24], and the homogeneous model. For the hot extreme of the database (T_{amb} > 30 °C, N = 196), the best overall performing correlation was Lockhart and Martinelli [19] with MAPE of 16.84% and an NRMSE of 20.45%. followed by the Wallis correlation [21]. Most models overpredict the experimental data during hot ambient temperature and underpredict the experimental data during cold ambient temperature. Nearly all correlations have higher predictability during cold ambient temperatures. An improved two-phase frictional pressure drop correlation is developed and proposed based on the Wallis correlation [21]. The MAPE, NRMSE, and predictability (±30% margin, all ambient temperatures) of the new correlation are of 16.84%, 20.45%, and 91.41%, respectively.

Acknowledgment

This material is based upon work financially supported by the U.S. National Science Foundation under Grant No. IIA-1301726.

Conflict of Interest

There are no conflicts of interest.

Data Availability Statement

The datasets generated and supporting the findings of this article are obtainable from the corresponding author upon reasonable request.

Nomenclature

Variables

f = friction factor
g = gravitational force, m/s^2
s = span
x = vapor quality
B = constant
C = constant
D = internal tube diameter, m
G = mass flux, kg/(m^2 s)
L = length, m
N = number of data points
P = pressure, kPa
T = temperature, °C
V = velocity, m/s
X = Lockhart-Martinelli parameter
$\dot{m}$ = mass flowrate, kg/s
E_i = error
Fr = Froude number
PE_i = percentage error, %
Re = Reynolds number

Greek Symbols

α = void fraction
Γ = Chisholm parameter
ε = roughness height, m
μ = dynamic viscosity, kg/(m s)
ρ = density, kg/m^3
σ = surface tension, N/m
ϕ = two-phase multiplier
ω = fan speed, Hz

Subscripts

a = air
amb = ambient
e = exit
exp = experimental
$fric$ = frictional
h = homogeneous
i = inlet
l = liquid
lo = liquid-only
lv = liquid-vapor
mod = model
mom = momentum
sat = saturation
$stat$ = static
$strat$ = stratified
$total$ = total
tp = two-phase
$tube$ = condensation tube
v = vapor

References

[1] Mahvi, A. J., Rattner, A. S., Lin, J., and Garimella, S., 2018, "Challenges in Predicting Steam-Side Pressure Drop and Heat Transfer in Air-Cooled Power Plant Condensers," Appl. Therm. Eng., **133**, pp. 396–406.
[2] Bracken, N., Macknick, J., Tovar-hastings, A., Komor, P., Gerritsen, M., Mehta, S., Bracken, N., Macknick, J., Tovar-hastings, A., and Komor, P., 2015, *Concentrating Solar Power and Water Issues in the U.S. Southwest*, M. Gerritsen, and S. Mehta, eds.
[3] Lips, S., and Meyer, J. P., 2012, "Experimental Study of Convective Condensation in an Inclined Smooth Tube. Part I: Inclination Effect on Flow Pattern and Heat Transfer Coefficient," Int. J. Heat Mass Transfer, **55**(1–3), pp. 395–404.
[4] Adelaja, A. O., Dirker, J., and Meyer, J. P., 2017, "Experimental Study of the Pressure Drop During Condensation in an Inclined Smooth Tube at Different Saturation Temperatures," Int. J. Heat Mass Transfer, **105**(1–3), pp. 237–251.
[5] Noori Rahim Abadi, S. M. A., Mehrabi, M., and Meyer, J. P., 2018, "Prediction and Optimization of Condensation Heat Transfer Coefficients and Pressure Drops of R134a Inside an Inclined Smooth Tube," Int. J. Heat Mass Transfer, **124**, pp. 953–966.
[6] Ewim, D. R. E., and Meyer, J. P., 2019, "Pressure Drop During Condensation at Low Mass Fluxes in Smooth Horizontal and Inclined Tubes," Int. J. Heat Mass Transfer, **133**, pp. 686–701.
[7] Zendehboudi, A., and Li, X., 2017, "A Robust Predictive Technique for the Pressure Drop During Condensation in Inclined Smooth Tubes," Int. Commun. Heat Mass Transfer, **86**(June), pp. 166–173.
[8] Kang, H. C., and Kim, M. H., 1994, "Effect of Non-Condensable Gas and Wavy Interface on the Condensation Heat Transfer in a Nearly Horizontal Plate," Nucl. Eng. Des., **149**(1), pp. 313–321.
[9] Dalkılıç, A. S., Çebi, A., Acikgoz, O., Wongwises, S., Dalkilic, A. S., Çebi, A., Acikgoz, O., Wongwises, S., Dalkılıç, A. S., Çebi, A., Acikgoz, O., and Wongwises, S., 2017, "Prediction of Frictional Pressure Drop of R134a During Condensation Inside Smooth and Corrugated Tubes," Int. Commun. Heat Mass Transfer, **88**, pp. 183–193.
[10] Xu, Y., and Fang, X., 2013, "A New Correlation of Two-Phase Frictional Pressure Drop for Condensing Flow in Pipes," Nucl. Eng. Des., **263**, pp. 87–96.
[11] Müller-Steinhagen, H., and Heck, K., 1986, "A Simple Friction Pressure Drop Correlation for Two-Phase Flow in Pipes," Chem. Eng. Process. Process Intensif., **20**(6), pp. 297–308.
[12] Kim, S. J., and No, H. C., 2000, "Turbulent Film Condensation of High Pressure Steam in a Vertical Tube," Int. J. Heat Mass Transfer, **43**(21), pp. 4031–4042.
[13] Carey, V. P., 1992, *Liquid Vapor Phase Change Phenomena: An Introduction to the Thermophysics of Vaporization and Condensation Processes in Heat Transfer Equipment*, CRC Press, New York, NY.
[14] Didi, M. B. O., Kattan, N., and Thome, J. R., 2002, "Prediction of Two-Phase Pressure Gradients of Refrigerants in Horizontal Tubes ´ Vision Des Gradients de Pression Des Frigorige ` Nes En Pre ´ Coulement Diphasique Dans Des Tubes Horizontaux E," Int. J. Refrig., **25**(7), pp. 935–947.
[15] Grönnerud, R., 1972, "Investigation of Liquid Hold-up, Flow-Resistance and Heat Transfer in Circulation Type Evaporators, Part IV: Two-Phase Flow Resistance in Boiling Refrigerants," Bull. l'Inst. Du Froid, Annex., 1.
[16] Wang, Y., Shen, S., and Yuan, D., 2017, "Frictional Pressure Drop During Steam Stratified Condensation Flow in Vacuum Horizontal Tube," Int. J. Heat Mass Transfer, **115**, pp. 979–990.
[17] Lips, S., and Meyer, J. P., 2012, "Experimental Study of Convective Condensation in an Inclined Smooth Tube. Part II: Inclination Effect on Pressure Drops and Void Fractions," Int. J. Heat Mass Transfer, **55**(1–3), pp. 405–412.
[18] Lips, S., and Meyer, J. P., 2011, "Two-Phase Flow in Inclined Tubes With Specific Reference to Condensation: A Review," Int. J. Multiph. Flow, **37**(8), pp. 845–859.
[19] Lockhart, R. W., and Martinelli, R. C., 1949, "Proposed Correlation of Data for Isothermal Two-Phase, Two-Component Flow in Pipes," Chem. Eng. Prog., **45**(1), pp. 39–48.
[20] Chisholm, D., 1967, "Lockhart-Martinelli Basis for the Correlation Flow for Two-Phase," Int. Commun. Heat Mass Transfer, **10**(18), pp. 1767–1778.
[21] Wallis, G. B., 1969, *One Dimensional Two-Phase Flow*, McGraw-Hill, New York.
[22] Steiner, D., 1993, *Heat Transfer to Boiling Saturated Liquids*, VDI-Warmeatlas (VDI Heat Atlas).
[23] Chisholm, D., 1973, "Pressure Gradients Due to Friction During the Flow of Evaporating Two-Phase Mixtures in Smooth Tubes and Channels," Int. J. Heat Mass Transfer, **16**(2), pp. 347–358.
[24] Friedel, L., 1979, "Improved Friction Pressure Drop Correlations for Horizontal and Vertical Two Phase Pipe Flow," European Two-Phase Flow Group Meeting, Ispra, Italy, pp. 485–491.
[25] El Hajal, J., Thome, J. R., and Cavallini, A., 2003, "Condensation in Horizontal Tubes, Part 1: Two-Phase Flow Pattern Map," Int. J. Heat Mass Transfer, **46**(18), pp. 3349–3363.